THE JOURNAL OF PHYSICAL CHEMISTRY B

Article

pubs.acs.org/JPCB

Atomic Mobility in a Polymer Glass after Shear and Thermal Cycles

Yongchul G. Chung and Daniel J. Lacks*

Department of Chemical Engineering, Case Western Reserve University, Cleveland, Ohio 44106, United States

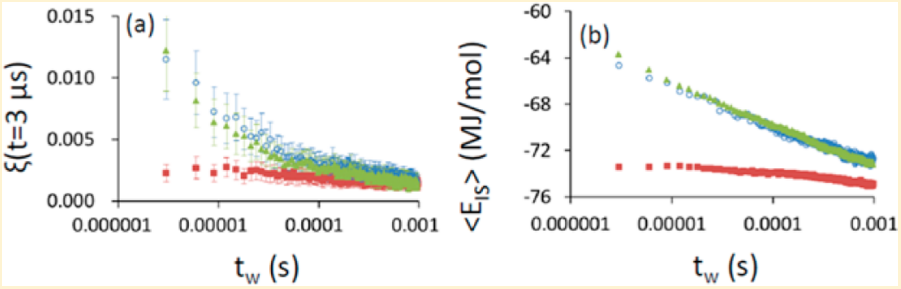

ABSTRACT: Molecular dynamics simulations and energy landscape analyses are carried out to study the atomic mobility of a polymer glass during the physical aging process that follows shear and thermal cycles. The mobility is characterized by the fraction of atoms moving more than their diameter in a given time interval. The mobility is enhanced after a shear or thermal cycle, and this enhancement decays with time. These mobility results are related to the position of the system on the energy landscape, as characterized by the average energy of the energy minima visited by the system; the mobility over longer time scales increases with the average energy of the energy minima visited, but the mobility over shorter time scales does not show a correlation with this average energy. From these results, we conclude that barriers separating metabasins composed of proximate energy minima, rather than barriers between individual energy minima, control the physical aging process. We also show that, after some finite time, the mobility following shear and thermal cycle appears to behave similarly to the mobility without perturbations; however, the system is at different regions of the energy landscape in these two cases, which implies that mobility alone does not characterize the state of the system.

1. INTRODUCTION

Glass-forming liquids (such as polymers) retain rigidity upon rapid cooling. Below its glass transition temperature (T_g), the atomic mobility of the liquid is frozen on the time scale of experiments, and this difference in the atomic mobility distinguishes glasses from liquids. Glasses are not at equilibrium, so their structures change slowly over time, which leads to a slow evolution of their bulk properties; this process is called physical aging (or structural relaxation). Elucidating the physical aging process in glasses is a major challenge in condensed matter physics due to its broad implications in both current and developing technologies.[1]

One approach to understanding physical aging is from the standpoint of potential energy landscape (PEL), which has been useful in describing dynamics of liquids and glasses.[2−4] The PEL consists of a large number of mechanically stable local minima ("inherent structures") of varying depths and saddle points ("barriers") that separate these minima. Additional topological properties of the PEL have been recently revealed: First, the barrier heights between minima become larger as the system moves toward the lower-energy regions of the PEL.[5,6] Second, groups of proximate local minima form superstructures on the PEL called "metabasins",[7,8] corresponding to a hierarchical topological ordering of local minima on the PEL. It has been shown that the mobility correlates with the PEL in that the average waiting time in the metabasins is inversely related to the diffusion coefficient.[9,10]

These properties of the PEL can be used to explain the surprising enhancement in atomic mobility of glasses under mechanical deformation, which has been observed in recent experiments[11,12] and simulations.[13,14] For example, the mobility enhancements following the cessation of deformation could be due to deformation moving the system to regions of the PEL with lower barriers.[15,16] With lower barriers, there will be more frequent transitions between energy minima, and thus higher mobility.

In this paper, we address the physical aging process following external perturbations. We quantify the atomic mobility over a range of time-scales, and relate these results to the system's position on the PEL. From these results, we propose that the dynamic results could be explained by considering the hierarchical ordering of the PEL, where the height of a barrier between metabasins depends on the system's position on the PEL but not necessarily the height of barriers between energy minima within a metabasin.

2. COMPUTATIONAL METHODS

Molecular dynamics (MD) simulations and energy landscape analyses are carried out to address the relationship between the system's mobility and its position on the PEL.

Received: October 2, 2012
Revised: November 14, 2012
Published: November 14, 2012

ACS Publications © 2012 American Chemical Society

dx.doi.org/10.1021/jp309772f | J. Phys. Chem. B 2012, 116, 14201−14205

a. Model. We used the coarse-grained (CG) model of atactic polystyrene (aPS) developed by Kremer and co-workers.[17−20] The CG model includes bond stretching, angle bending, torsion, and intrachain interactions parametrized so that the bulk properties (e.g., diffusion coefficient and density) of polystyrene derived from the simulation results match those of fully atomistic simulations. When compared to earlier polymer models (e.g., the Kremer−Grest model,[21] which incorporates only nonbonded interactions and simple harmonic potentials for bonded interactions), the additional contributions produce more realistic results and thus are more relevant to interpreting experimental results. The physical time in the CG model is obtained by scaling the simulation time by a scale factor determined in comparison between the all-atomic model and the coarse-grained model. The scale factor ranges from 500 to 5000, depending on molecular weight, density, and temperature,[19] but for simplicity, we use a constant scale factor of 1000. All times reported in this paper are physical times (i.e., after the scaling factor has been applied).

The simulations are carried out for a system of 50 aPS chains, where each chain is composed of 192 monomer units. A styrene monomer for the CG model is mapped onto two types of superatoms: type A (representing the styrene backbone), and type B (representing phenyl ring group). A large system size (N = 19,200 atoms) was chosen to more closely approximate a macroscopic system.

b. Molecular Simulations. We carry out several sets of MD simulations. Periodic boundary conditions are imposed in all directions. The Berendsen thermostat is used to control the system temperature. For the constant-pressure simulations (NPT ensemble), the pressure is controlled by the Berendsen barostat; all NPT simulations are carried out at a pressure of 1 bar. The Leapfrog method is used to numerically integrate the equations of motion with a time step of 3 ps (after scaling). All simulations are carried out using the GROMACS 4 package.[22]

First, we carry out a set of simulations to address the glass transition behavior. These simulations begin with equilibrated systems at T = 503 K, and then instantaneously cool the system to a target temperature T by resetting the thermostat temperature. A 30 μs NPT simulation is run at each T. The target temperatures range from T = 283 K to T = 483 K, in 20 K intervals.

Second, a series of MD simulations are run to slowly cool the system to T = 300 K. This procedure starts with a 30 μs NPT simulation at T = 503 K. After instantaneous cooling to T = 363 K under NPT (which is slightly below T_g, so that there's still some atomic mobility), a 102 μs simulation is run at T = 363 K with constant volume. A second instantaneous cooling step is then carried out, and a 30 μs NPT simulation is run at T = 300 K. The outputs of these simulations are used as the starting points for our studies. In regard to this cooling protocol, we note that any cooling protocol in MD simulations is artificial, because the thermostats used to control the temperature are nonphysical. We feel that instantaneous changes followed by constant-temperature runs have the advantage of being less ambiguous, since the artificial thermostats may play less of a role with this protocol.

Starting from these slowly cooled systems at T = 300 K, we apply mechanical and thermal perturbations and examine the relaxation after the perturbation. The perturbations are intentionally applied very fast so that little relaxation occurs during the perturbation process; i.e., the shear rate used for the mechanical perturbation is very high, and the temperature changes used for the thermal perturbation are instantaneous. After the perturbations, long MD simulations for 1002 μs were carried out at constant volume.

For the mechanical perturbation, shear is applied with the Lees−Edwards boundary conditions in the xy-plane of the simulation cell; this procedure shifts an element of the simulation cell at a constant rate. We impose a cycle of shear deformation consisting of 200% forward shear and then 200% backward shear, at the shear rate $\dot{\gamma} = 1.7 \times 10^7$ s^{-1} (this high shear rate was chosen so that little relaxation occurs during the shearing process; note that we addressed the effects of shear rate previously[16]). After this cycle of shear, we run 10 independent MD simulations, where each simulation is run for 1002 μs.

For the thermal perturbation, we instantaneously increase the system temperature to T = 503 K, run a 3 μs simulation at constant volume, and then instantaneously decrease the temperature back to T = 300 K. After this thermal cycle, we run 10 independent MD simulations, where each simulation is run for 1002 μs.

In addition, we carried out a control case, where the long MD simulation is run without a perturbation. In this case, we run 10 independent MD simulations, where each simulation is run for 1002 μs.

The energy landscape analysis is carried out by minimizing the potential energy of the system starting from configurations obtained during the MD simulations. The configurations are extracted after the MD simulations are completed; therefore, these energy minimizations do not affect the atomic trajectories during the MD simulations. The depths of the energy minima visited during MD simulations ("inherent structure energies", E_{IS}) are calculated using the l-bfgs algorithm,[23−25] and are considered complete when the largest force in the system becomes less than 10^{-7} N. Results for the quench, sheared, and control systems are averaged over 10 independent runs.

c. Analysis. We quantify the atomic mobility in the system using the one-dimensional van Hove function. The van Hove function is the probability of a particle displacement of magnitude z during time interval t and can be expressed as

$$G_s(z, t) = \frac{1}{N}\sum_{i=1}^{N} \delta(z - |z_i(t_w + t) - z_i(t_w)|) \quad (1)$$

where z_i is the z-coordinate of particle i, N is the number of particles, and t_w is the time when the measurement starts which we refer to as the waiting time. Note that results are shown only for particles of type B (similar results are obtained for particles of type A), the van Hove function depends on t_w because out-of-equilibrium systems are being examined, and the z direction is chosen because it is perpendicular to the plane of applied shear. We examined the atomic mobility in the system for time intervals ranging from t = 0.3 to 30 μs.

We further quantify the atomic mobility by defining $\xi(t)$, the probability that a particle moves more than 5 Å in time t; $\xi(t)$ is obtained by integrating $G(z, t)$ from 5 Å to ∞. Note that this cutoff distance is approximately one particle diameter (σ = 5.2 Å for particles of type B), and thus an atom moving more than this cutoff distance corresponds to an escape from its cage of neighbors.

3. RESULTS

We first examine the average inherent structure energy ($\langle E_{IS} \rangle$) of the system as a function of temperature, and these results are

shown in Figure 1. $\langle E_{IS}\rangle$ decreases with decreasing temperature, because as the kinetic energy decreases, the system becomes

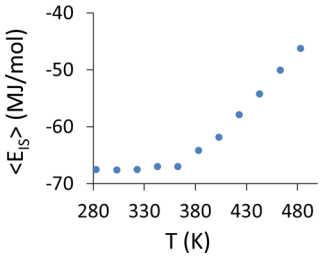

Figure 1. The average inherent structure energy, $\langle E_{IS}\rangle$, as a function of temperature.

increasingly confined to the lower-energy regions on the PEL.[5] However, below a certain temperature, the value of $\langle E_{IS}\rangle$ no longer decreases with decreasing temperature (on the time scale of these simulations); this temperature corresponds to T_g. The T_g value obtained from this method ($T_g \approx 370$ K) is similar to the value obtained from other properties ($T_g \approx 380$ K by changes in volume[26]) as well as from experiments ($T_g \sim 368$ K[27]). We note that the system is out of equilibrium below T_g, and will slowly move to lower energy regions of the PEL by the physical aging process.

The van Hove functions at various temperatures are shown in Figure 2a, for time increment t = 3 μs. The van Hove

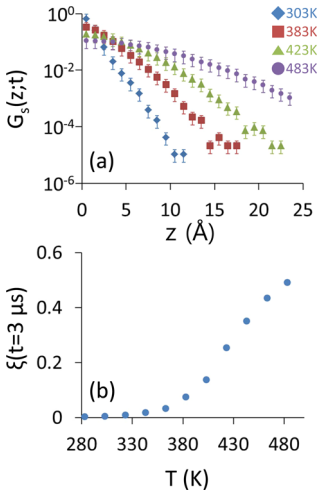

Figure 2. (a) Results for the van Hove function in the z-direction for fixed time interval (t=3 μs) at various temperatures. (b) The probability that an atom moves more than 5 Å, $\xi(t)$, as a function of temperature.

function in the out-of-equilibrium system depends on the time the measurement is taken (t_w); for consistency in Figure 2a, we use t_w = 27 μs. The tail of the van Hove function becomes more stretched with increasing temperature, indicating that the atoms are moving further during this time increment with the increased kinetic energy. This effect is further quantified with $\xi(t$=3 μs), the probability that an atom moves a distance greater than 5 Å during t = 3 μs (Figure 2b). Figure 2b shows that $\xi(t$=3 μs) increases nearly linearly for temperatures above T_g. The value of $\xi(t$=3 μs) also captures the glass transition behavior—as the system's temperature decreases below T_g, the value of $\xi(t$=3 μs) deviates from the linear curve and approaches zero.

The temperature dependence of $\xi(t$=3 μs) (Figure 2b) is similar to the temperature dependence of $\langle E_{IS}\rangle$ (Figure 1), and the relationship between these properties is shown in Figure 3.

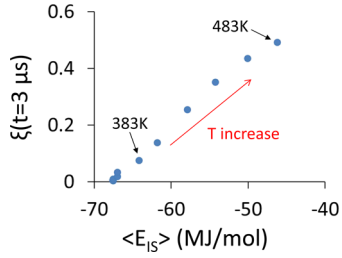

Figure 3. $\xi(t$=3 μs) as a function of $\langle E_{IS}\rangle$. Each point corresponds to a different temperature (in temperature increments of 20 K).

The results show that the system's dynamics are strongly correlated to its position on the energy landscape; i.e., faster dynamics occur when the system is at higher-energy regions on the PEL.

We examine the system behavior following two types of perturbations: a shear cycle (200% shear forward then 200% shear backward) and a thermal cycle (temperature increased above T_g then back to 300 K). For a control case, we allow the system to evolve without any perturbation. We quantify the dynamics in these systems using $\xi(t)$ and the position of these systems on the PEL using $\langle E_{IS}\rangle$.

The van Hove function results from these simulations are shown in Figure 4. The dynamics exhibit enhanced mobility (in

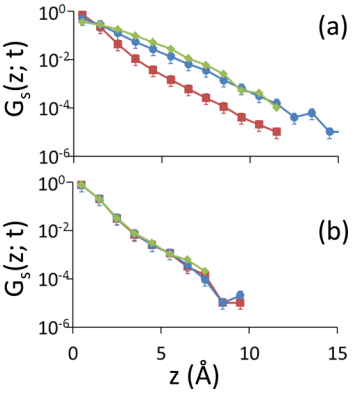

Figure 4. Results for the van Hove function in the z-direction with t = 3 μs for thermal cycle (green, △), shear cycle (blue, ●), and control (red, ■) system at (a) t_w = 0 μs and (b) t_w = 900 μs.

comparison to the control case), as identified by longer tails of the van Hove function, immediately after the shear or thermal perturbation (Figure 4a). However, the enhanced mobility fades away with time, as shown by the results at t_w = 900 μs (Figure 4b). The change in the mobility with time is shown in Figure 5a, as quantified by $\xi(t$=3 μs). We see the results for $\xi(t$=3 μs) for the shear and thermal cycles follow similar trajectories during the relaxation process.

The results for $\langle E_{IS}\rangle$ during these simulations are shown in Figure 5b. Since the system volume is the same in all cases, the underlying PEL is also the same. These results show that both the shear and thermal cycles move the system to higher energy regions on the PEL, and that $\langle E_{IS}\rangle$ evolves in a similar manner for both the shear and thermal cycles. We note that while the $\xi(t$=3 μs) for the perturbed cases appear to converge to the

dx.doi.org/10.1021/jp309772f | J. Phys. Chem. B 2012, 116, 14201−14205

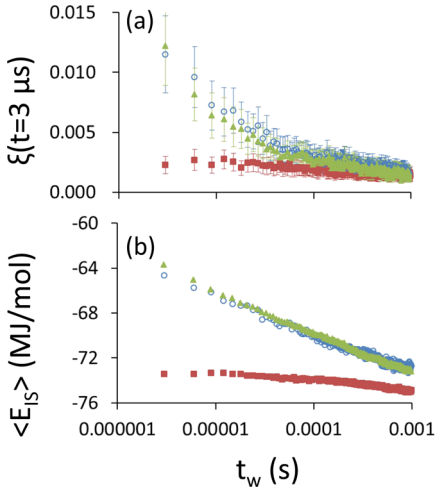

Figure 5. (a) $\xi(t{=}3\ \mu s)$; (b) the inherent structure energy, $\langle E_{IS}\rangle$, as a function of different waiting times (t_w). Results are for thermal cycle (green, △), shear cycle (blue, ●), and control (red, ■).

control case by 1000 μs, the values for $\langle E_{IS}\rangle$ for the perturbed cases remain significantly greater than that for the control case at this time.

Physical insight is gained by examining $\xi(t)$ as a function of $\langle E_{IS}\rangle$, for various time intervals t (Figure 6). For t = 0.3 μs (Figure 6a), the mobility depends only weakly on the position of the system on the PEL. However, for t = 3 and 30 μs (Figure 6b,c), the mobility depends strongly on the position on the landscape, such that the mobility is significantly greater when the system is in the higher energy regions of the landscape. This difference in behavior can be understood in terms of the cage

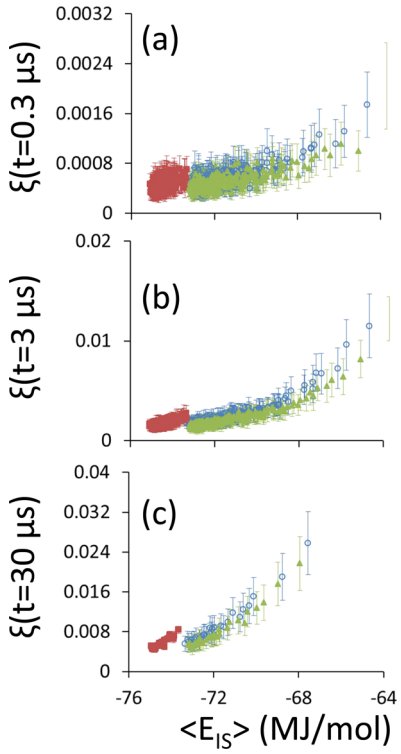

Figure 6. $\xi(t)$ as a function of E_{IS} for various t. Results are for quench (green, ◆), sheared (blue, ○), and unsheared (red, ■): (a) t = 0.3 μs; (b) t = 3 μs; (c) t = 30 μs.

escape picture of the mobility of atoms in a liquid or glass, wherein diffusive motion corresponds to an atom escaping the cage surrounded by its neighboring atoms. This cage behavior can be seen in a plot of the mean squared displacement (MSD), as shown in Figure 7—the plateau region corresponds to the

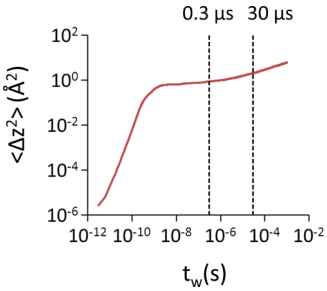

Figure 7. The mean squared displacement in the z-direction at T = 300 K for type B atom with t_w = 0 μs. These results are from the control simulation. The vertical dashed lines indicate the time scale corresponding to the measurement time, t.

time that atoms are trapped in their cages. The deviation of the MSD curve from the plateau indicates escape of atoms from their cages, so an *approximate* time scale for cage escape $\tau_{escape} \approx 0.1\ \mu s$ (for the control system at T = 300 K). Thus, the results in Figure 6 show that the mobility depends strongly on the position on the landscape for time intervals $t \gg \tau_{escape}$ but only weakly for $t \approx \tau_{escape}$. Note that our value for τ_{escape} is only approximate and intended to indicate the order of magnitude, and that our associated arguments are only qualitative.

This cage behavior is qualitatively attributed to metabasins of the PEL. The cage escapes discussed above correspond to irreversible diffusive motion. In contrast to this diffusive motion, atoms can reversibly rearrange by "rattling around" within a cage. This rattling around can correspond to both dynamics within a single energy minimum and to transitions between energy minima within a metabasin. When atoms escape a cage, this corresponds to a transition to a different metabasin. Therefore, our results in Figure 6 suggest that the position on the energy landscape affects the heights of barriers between metabasins but not of barriers within a metabasin. We acknowledge that this connection between cage dynamics and metabasins is qualitative.

4. DISCUSSION AND CONCLUSION

Our results elucidate the relationship between atomic mobility and the system's position on the energy landscape. A change in temperature leads to both a change in the system's position on the PEL (Figure 1) and a change in atomic mobility (Figure 2b). Figure 3 shows that these two properties are highly correlated; i.e., the atomic mobility becomes larger as the system explores higher energy regions on the PEL. However, the relationship between atomic mobility and the position on the PEL is more complex; in Figure 6, we show that the dependence of atomic mobility on $\langle E_{IS}\rangle$ is stronger at the higher energy regions than at lower energy regions. Furthermore, the dependence becomes more pronounced when the mobility is examined over longer time scales; for short time scales (e.g., t = 0.3 μs), there is little dependence of the mobility on $\langle E_{IS}\rangle$ except at very high $\langle E_{IS}\rangle$. Since the dependency of the mobility with respect to $\langle E_{IS}\rangle$ only appears when $t \gg \tau_{escape}$, we could understand that τ_{escape} increases as the system moves toward the lower energy regions of the PEL,

dx.doi.org/10.1021/jp309772f | J. Phys. Chem. B 2012, 116, 14201−14205

and this is the reason why atomic mobility (as quantified for $\xi(t)$) loses its dependency on $\langle E_{IS} \rangle$ as it moves toward lower energy regions of the PEL.

The relationship between the atomic mobility in the system and the system's position on the PEL can also be observed in the relaxation behavior following shear and thermal cycles. Experimentalists often use a thermal cycle to "rejuvenate" aged glasses, i.e., to recover material characteristics of its state prior to physical aging. It has been suggested that the mechanical deformation also leads to a similar rejuvenation.[28] A PEL description of "rejuvenation" is based on the fact that the physical aging moves the system toward lower energy regions on the PEL.[29] Since "rejuvenation" acts opposite to the physical aging process, it could be understood as moving the system to higher energy regions on the PEL. We show in Figure 5b that both shear and temperature cycles indeed move the system to higher energy regions on the PEL, and the atomic mobility changes accordingly (Figure 5a). Note that, in Figure 5, the evolutions of both $\langle E_{IS} \rangle$ and $\xi(t=3\ \mu s)$ are very much the same for the system under shear and thermal perturbations, and it is, therefore, tempting to conclude that these two types of perturbations affect the system in an identical way. However, we recently showed that the structural changes (as quantified by the torsion angle distribution) following thermal and mechanical perturbations are different.[26] For example, temperature increases always move the system to higher-energy torsional states, but shear deformation sometimes moves the system to lower-energy torsional states. These results suggest that the atomic mobility alone cannot be used to conclude that a shear cycle "rejuvenates" the system in the same way as a thermal cycle. We also note that the experimental results from McKenna and co-workers[30] (based on torsional dilatometric and calorimetric measurements) and simulation results from Lyulin and Michels[31] suggest that strain does not literally rejuvenate the material.

In summary, we examine the relationship between atomic mobility and the system's position on the PEL. We find that these properties are correlated only for certain positions on the PEL and certain time scales. The correlation exists for $t \gg \tau_{escape}$; since τ_{escape} is related to the barrier height separating metabasins on the PEL, we suggest that the barriers separating the metabasins are relevant features on the PEL that affect the dynamics during the physical aging process. Our results show that PEL features typical of simpler (nonpolymeric) glass formers are also relevant in polymer systems, which supports the generality of the PEL paradigm. Furthermore, we show that both thermal and shear cycle moves the system to higher energy regions on the PEL, and this repositioning of the system on the PEL is responsible for increased atomic mobility in the system. Following these perturbations, the enhanced mobility for both perturbations decays similarly, and a "*dynamic* rejuvenation" occurs with this shear cycle (but this rejuvenation is not apparent in all properties). Similar results have been shown in recent experiments with polymer glasses.[32] Finally, we note that the value of $\langle E_{IS} \rangle$ (which contains structural information of the system) does not reveal the difference between the glasses under different types of perturbations, and other measures (such as torsion angle[26]) must be used in order to reveal the differences in structure under these perturbations.

AUTHOR INFORMATION

Notes

The authors declare no competing financial interest.

ACKNOWLEDGMENTS

This work was funded by the National Science Foundation under the grant DMR-0705191. We thank Dominik Fritz and Kurt Kremer for their help with the coarse-grained molecular model, and the Ohio Supercomputer Center for providing the computational resources for the simulations carried out in this paper.

REFERENCES

(1) Ediger, M.; Harrowell, P. *J. Chem. Phys.* **2012**, *137*, 080901.
(2) Goldstein, M. *J. Chem. Phys.* **1969**, *51*, 3728−3739.
(3) Stillinger, F. H.; Weber, T. A. *Phys. Rev. A* **1982**, *25*, 978−989.
(4) Debenedetti, P. G.; Stillinger, F. H. *Nature* **2001**, *410*, 259−267.
(5) Sastry, S.; Debenedetti, P. G.; Stillinger, F. H. *Nature* **1998**, *393*, 554−557.
(6) Doliwa, B.; Heuer, A. *Phys. Rev. E* **2003**, *67*, 031506.
(7) Stillinger, F. H. *Science* **1995**, *267*, 1935−1939.
(8) Stillinger, F. H. *Phys. Rev. B* **1990**, *41*, 2409−2416.
(9) Büchner, S.; Heuer, A. *Phys. Rev. Lett.* **2000**, *84*, 2168−2171.
(10) Doliwa, B.; Heuer, A. *Phys. Rev. E* **2003**, *67*, 030501.
(11) Loo, L. S.; Cohen, R. E.; Gleason, K. K. *Science* **2000**, *288*, 116−119.
(12) Lee, H-.N.; Paeng, K.; Swallen, S. F.; Ediger, M. *Science* **2009**, *323*, 231−234.
(13) Capaldi, F. M.; Boyce, M. C.; Rutledge, G. C. *Phys. Rev. Lett.* **2002**, *89*, 175505.
(14) Warren, M.; Rottler, J. *Phys. Rev. Lett.* **2010**, *104*, 205501.
(15) Lacks, D. J.; Osborne, M. J. *Phys. Rev. Lett.* **2004**, *93*, 255501.
(16) Chung, Y. G.; Lacks, D. J. *Macromolecules* **2012**, *45*, 4416−4421.
(17) Harmandaris, V. A.; Adhikari, N. P.; van der Vegt, N. F. A.; Kremer, K. *Macromolecules* **2006**, *39*, 6708−6719.
(18) Mulder, T.; Harmandaris, V. A.; Lyulin, A. V.; van der Vegt, N. F. A.; Kremer, K.; Michels, M. A. J. *Macromolecules* **2009**, *42*, 384−391.
(19) Harmandaris, V. A.; Kremer, K. *Macromolecules* **2009**, *42*, 791−802.
(20) Fritz, D.; Harmandaris, V. A.; Kremer, K.; van der Vegt, N. F. A. *Macromolecules* **2009**, *42*, 7579−7588.
(21) Kremer, K.; Grest, G. S. *J. Chem. Phys.* **1990**, *92*, 5057−5086.
(22) Hess, B.; Kutzner, C.; van der Spoel, D.; Lindahl, E. *J. Chem. Theory Comput.* **2008**, *4*, 435−447.
(23) van der Spoel, D.; Lindahl, E.; Hess, B.; van Buuren, A. R.; Apol, E.; Meulenhoff, P. J.; Tieleman, D. P.; Sijbers, A. L. T. M.; Feenstra, K. A.; van Drunen, R.; Berendsen, H. J. C. *Gromacs User Manual version 4.5.4*, 2010; www.gromacs.org.
(24) Byrd, R. H.; Lu, P.; Nocedal, J. *SIAM J. Sci. Stat. Comput.* **1995**, *16*, 1190−1208.
(25) Zhu, C.; Byrd, R. H.; Nocedal, J. *ACM Trans. Math. Software* **1997**, *23*, 550−560.
(26) Chung, Y. G.; Lacks, D. J. *J. Chem. Phys.* **2012**, *136*, 124907.
(27) Zoller, P.; Walsh, D. *Standard PVT data for Polymers*, 1st ed.; CRC Press: Boca Raton, FL, 1995.
(28) Struik, L. C. E. *Physical aging in amorphous polymers and other materials*; Elsevier: New York, 1978.
(29) Kob, W.; Barrat, J.-L. *Phys. Rev. Lett.* **1997**, *78*, 4581−4584.
(30) McKenna, G. B. *J. Phys.: Condens. Matter* **2003**, *15*, S737−S763.
(31) Lyulin, A.; Michels, M. A. J. *Phys. Rev. Lett.* **2007**, *99*, 085504.
(32) Lee, H.-N.; Ediger, M. D. *Macromolecules* **2010**, *43*, 5863−5873.